RSC Advances

PAPER

View Article Online
View Journal | View Issue

Cite this: *RSC Adv.*, 2017, **7**, 32552

Self-driven mercury motor *via* redox reaction in acid solution†

Jiali Wang,[a] Baozhan Zheng,[a] Jinlan Xiao,[b] Xiaoling Liu,[a] Hongyun Ji,[b] Juan Du,[a] Yong Guo*[a] and Dan Xiao *[ab]

Received 24th April 2017
Accepted 10th June 2017

DOI: 10.1039/c7ra04574c

rsc.li/rsc-advances

Recently, the deformation of liquid metals and self-driven liquid metal motors have received extensive close attention because of their wide applications. The construction of self-driven motors is based on the conversion of chemical energy into mechanical energy. Here, the reversible deformation of a mercury drop in $NaIO_4$ solution was investigated. The self-driven motion of a mercury drop in $NaIO_4/H_2SO_4$ solution was demonstrated for the first time. The mercury drop was oxidized in $NaIO_4$ solution, and then contacted with a metal foil swimming in an acid environment. The average speed of the mercury motor is 10 cm s^{-1}, which is faster than previously reported. The effects of the pH and the concentration on the movement were investigated. Besides, some interesting phenomena, such as pushing, colliding and bouncing between the mercury motor and the mercury drop, were investigated. We present the mechanism of self-driven motion and interaction between two mercury drops. The results demonstrate that the phenomenon should be attributed to the charge transfer, which caused the pressure difference on two ends of the mercury drop. These results have important significance for pressure sensing, mass transfer and the development of intelligent robots.

1 Introduction

The autonomous locomotion of droplets has attracted great interest over the past few decades. Up to now, many motors have been reported and applied in drug delivery[1,2] and smart sensors.[3,4] These motors rely on external energy to make themselves turn into an asymmetric state and move in solution, including water,[5,6] acids,[7] bases,[8] hydrogen peroxide.[9,10] However, it is still a challenge to convert external energy[11,12] into kinetic energy for macroscopic motors because the external energy is unstable. These motors will be affected once the external energy is altered or inaccessible. A self-driven motor can spontaneously convert chemical energy into kinetic energy to induce autonomous locomotion without external energy. Liquid metals have received extensive attention for their unique property of softness, which holds great promise in making flexible motors.[13] Compared with traditional motors,[14–16] liquid metal motors have the flexibility of a liquid and the characteristics of metal, which makes them competent to perform special missions under tough conditions.

Recently, the deformation of a liquid metal based on gallium under the action of an electric field was reported.[11,17–21] The reversible deformation of the liquid metal between spherical and irregular was realized under electrochemical oxidation and dissolution, which were the prerequisites for the self-driven motor. Besides, liquid metal motors driven by external energy have also been studied. Typically, external physical energy from the surrounding electromagnetic field,[12] electric field[22,23] or light[24] is employed to transform into mechanical energy. A motor based on liquid metal eating Al in NaOH solution moved autonomously with a relatively constant velocity of 5 cm s^{-1}, which is a huge step forward for the development of self-driven motors. Subsequently, a new method for accelerating the movement of liquid metal was demonstrated in acid solution. The liquid metal droplets achieved a relatively fast speed through a liquid medium and along predefined metallic paths.[25] The driving of the liquid metal by redox was also studied, which was actually equivalent to the deformation of liquid metal.[21] The mercury beating heart system was first reported by Lippmann,[26] in which a mercury drop sustained a beat in $K_2Cr_2O_7/H_2SO_4$ solution. The coupling phenomenon of the mercury heartbeat (MBH) system[27] and the deformation of mercury under the action of an electric field have been studied,[28,29] which led to the deepening of the initial mercury breathing phenomenon.

Previous reports of self-driven motors were focused on gallium indium alloys, which need a fusion process of gallium and aluminium foil, and the system for the self-driven motor is

[a]College of Chemistry, Sichuan University, 29 Wangjiang Road, Chengdu, 610064, China. E-mail: guoy@scu.edu.cn; Fax: +86-28-85412907; Tel: +86-28-85416218
[b]College of Chemical Engineering, Sichuan University, 29 Wangjiang Road, Chengdu 610064, China. E-mail: xiaodan@scu.edu.cn; Fax: +86-28-85415029; Tel: +86-28-85416029

† Electronic supplementary information (ESI) available. See DOI: 10.1039/c7ra04574c

an alkaline environment. Besides this, as far as we know, there are no reports of self-driven mercury motors in acid solution. Inspired by previous work, we studied the self-driven mercury motor and the interaction between two mercury drops in $NaIO_4$/H_2SO_4 solution. The motion mechanism of the self-driven mercury motor were discussed. In this work, the actuation mechanism is not exactly the same as in previous reports.

2 Experiments

2.1 Experimental materials

Sodium periodate ($NaIO_4$) was chemically pure and was used as the oxidizing agent without purification. 98% H_2SO_4 solution was of analytical grade and was commercially obtained from Chain Medicine OM. Deionized water was used for testing experiments. Mercury was covered by an aqueous solution of sulfuric acid and an oxidizing agent solution. All safety recommendations on the handling of mercury were met.

2.2 Preparation of solutions

Electrolyte solutions were prepared using deionized (DI) water, 0.05 M $NaIO_4$ solution and 0.2 M H_2SO_4. The pH was measured by pH meter (Ray Magnetic PHS-3c acidity meter).

2.3 The deformation of the mercury drop

A mercury droplet was placed in a weighing bottle (40 × 25 mm), which was filled with electrolyte solutions. 1 mL of 0.05 M $NaIO_4$ in deionized water was added to form the electrolyte used for the deformation experiment. Plastic tweezers were used for the deformation. Three separated mercury drops were prepared in the weighing bottle (40 × 25 mm), which was filled with 10 mL deionized water and 0.5 mL $NaIO_4$ (0.05 M) solution. AN iron nail was immersed in solution and attached to the mercury drops. Then the phenomena of the mercury drops was observed and recorded.

2.4 Synthesis of self-driven mercury motor

The designed self-driven motor in this work was made up of a mercury drop and metal foil (aluminium foil and copper foil) in $NaIO_4$/H_2SO_4 solution. Here, the copper foil and aluminium foil were used as fuel.

pH of solution. A mercury droplet was placed in a Petri dish with 10 mL of deionized water and 1 mL of $NaIO_4$ solution, then acid was added to adjust the pH from 7 to 1. Then the metal foil (copper foil and aluminium foil) was connected with the mercury and the movement of the droplets was observed.

Volume of mercury drop. Using the above solution and experimental process, we used different size mercury droplets ($D = 2$ mm, $D = 3.5$ mm) as the research object and observed the velocity of the droplet.

Volume of $NaIO_4$ solution. A mercury droplet was placed in a Petri dish with 10 mL of deionized water. We added acid to adjust the pH to 2.3 and added 0.1 mL of 0.05 M $NaIO_4$ every time to the solution. Then the aluminium foil was connected with the mercury and the movement of the droplets was observed.

Temperature of solution. A mercury droplet was placed in a Petri dish with 10 mL of deionized water and 1 mL of $NaIO_4$ solution, then acid was added to adjust the pH to 2.3. Then the aluminium foil was connected with the mercury. The temperature of the solution was regulated using an ice salt bath. The speed of the mercury motor was recorded.

2.5 The interaction between the mercury motor and the mercury drop

We injected a mercury drop to the self-driven mercury motor system, and then observed the phenomena between them.

3 Results and discussion

3.1 Deformation phenomenon of mercury drop in $NaIO_4$ solution

First, we observed the deformation and merging of the mercury drop. We put the mercury drop in a glass container with deionized water to make sure that the mercury drop was covered by deionized water. When $NaIO_4$ solution was added to the above-mentioned solution, it was found that the metallic luster of mercury disappeared and the shape of the mercury transformed from its original sphere into a flat one. The surface tension of the mercury drop was decreased by oxidation. Subsequently, the mercury drop was easy to change into an irregular shape by poking with plastic tweezers, which indicates that the shape of the mercury drop was affected by significant variations of the surface tension. The snapshots of the irregular shape of the mercury are shown in Fig. 1A. When separated mercury drops were prepared, it was discovered that the iron nail merged these separate metal spheres into a larger sphere in the solution. Fig. 1B presents the original separated mercury droplets and the merging process. Following the schematic procedures outlined in Fig. 1C, three independent mercury drops were deposited on the bottom of the Petri dish close to

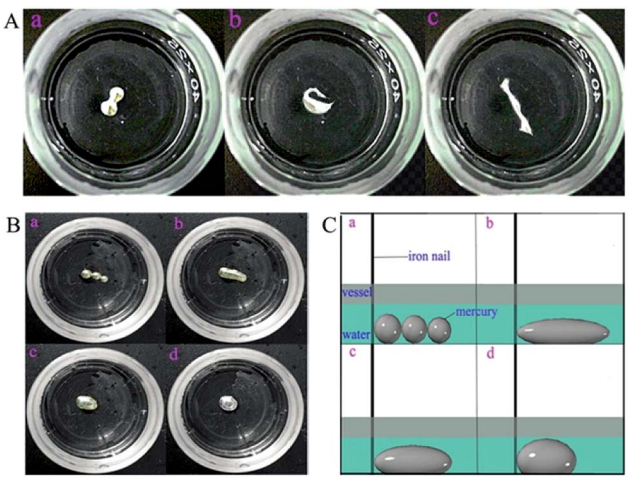

Fig. 1 Photographs of the transformation and merging of liquid metal objects. (A) Snapshots of liquid metal transformation from spherical into irregular shape. (B) Snapshots of the combination of three separated mercury droplets. (C) Schematic of the combination of three separate mercury droplets.

each other in a row. The iron nail was immersed in solution and attached to the mercury drops. It was observed that these independent mercury droplets merged into a long strip in the solution. The nail remained close to the liquid metal, and then the long strip was transformed into a spherical shape. Moreover, the liquid metal surface was changed from gloomy to metallic luster. According to the theory of interfacial phenomenon, the surface tension controls the shape of the mercury droplet in solution.[30,31] Surface tension is an inherent properties for liquid metals and external conditions can impact it. Analytically, the mercury drop was oxidized and a thin layer of mercury oxide was produced when we added the $NaIO_4$ solution to deionized water. The formation of a thin oxide layer led to a decrease of the mercury drop's surface tension. Therefore, the shape of the mercury was affected by $NaIO_4$ solution without any external energy. The merging of the original separate mercury droplets indicated that the nail played an important role.

According to the theory of free electrons, there are free electrons on the surface of the nails. When the nails were close to the mercury drops, electrons were transferred from the nail to the surface of the mercury, and the quantity of electric charge on the surface of the mercury was changed (the oxide layer on the surface of the mercury drop was reduced by receiving electrons), which promoted the amalgamation of mercury droplets. Thus, the above merging was mainly governed by the changes in surface tension owing to electron transfer. The charge distribution in the process of mercury droplet merging is shown Fig. 2.

3.2 Self-driven mercury motor

Herein, we designed a motor with mercury and metal foils in $NaIO_4/H_2SO_4$ solution. Fig. 3A exemplifies a mercury motor

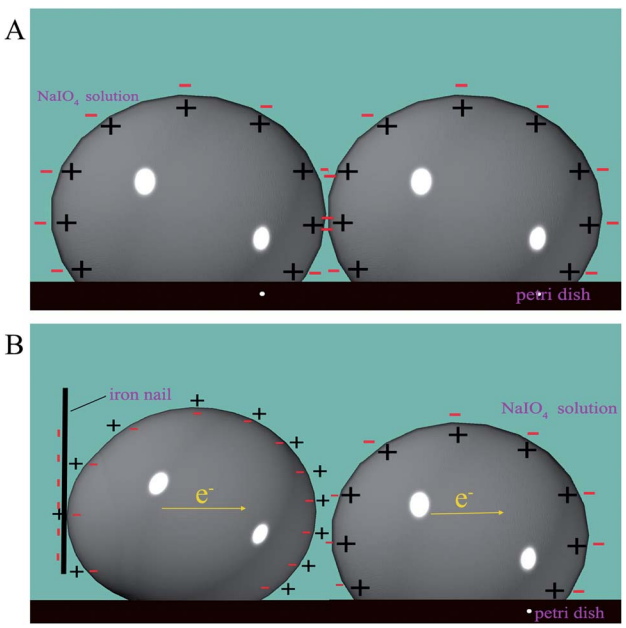

Fig. 2 The charge distribution in the process of mercury droplet merging. (A) Schematic of charge distribution of two mutually independent and close mercury droplets in $NaIO_4$ solution. (B) Schematic of the nail's influence on the charge distribution of two mutually independent and close mercury droplets in $NaIO_4$ solution.

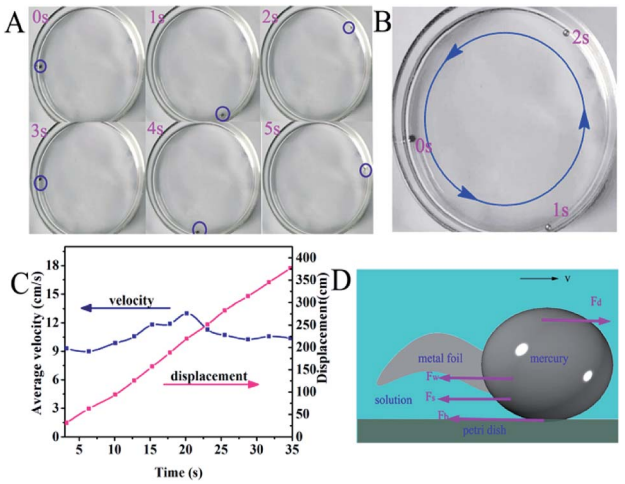

Fig. 3 Photographs of the self-driven motor moving in the container. (A) Spatiotemporal evolution of a droplet ($D = 2$ mm) in a Petri dish. (B) The self-driven motor ($D = 2$ mm) moves along the wall of the Petri dish. (C) Time–average velocity and time–displacement plots within 35 s for the mercury motor. (D) Schematic of forces affecting the velocity of the motor.

swimming autonomously in a circular Petri dish (ESI Movies S1 and S2†). Here, we used aluminium foil as the fuel because the driven speed of the Hg/Al motor was faster than that of the Hg/Cu motor (ESI Movies S3 and S4†). The mercury drop began to move immediately with a quick speed along the wall of the Petri dish when it contacted with the aluminium foil (Fig. 4 and ESI Movie S5†). The velocity and displacement of this motor within 35 s (about 12 laps) are depicted in Fig. 3C. According to the free electron theory of metals, the interaction between the nucleus of the metal atom and its valence electrons is weak, valence electrons can easily become free electrons which makes the cations accumulate nearby and form an electric double layer (EDL) on the surface of the mercury drop (Fig. 5A). After adding $NaIO_4$ into the solution, the mercury droplet was oxidized, which changed the shape and electric double layer (EDL) of the mercury drop (Fig. 5B). After putting aluminium foil into the $NaIO_4$ solution, an oxidation layer was formed on the surface, and the transfer of electrons from the Al to the mercury drop was prevented owing to the oxidation layers on the surface of Al (Fig. 5C); therefore, the mercury drop cannot move in this condition. We added a drop of H_2SO_4 to the solution. The mercury drop with aluminium foil began to spontaneously move without any external energy. It can be seen that the shape of the mercury was recovered to a certain degree. We speculated that the mercuric oxide and alumina reacted with H_2SO_4, and the decrease of the oxide layer accelerated the electron transfer from the aluminium foil to the mercury, which caused the motor to move immediately. Therefore, the dissolution and formation of the oxide layer reached a dynamic equilibrium in $NaIO_4/H_2SO_4$ solution (Fig. 5D and E).

The forces on the mercury drop were analysed (Fig. 4C) in order to further investigation of the movement. Theoretically, there are two kinds of force present on the mercury drop: one of the forces was driving and another was resistance, which

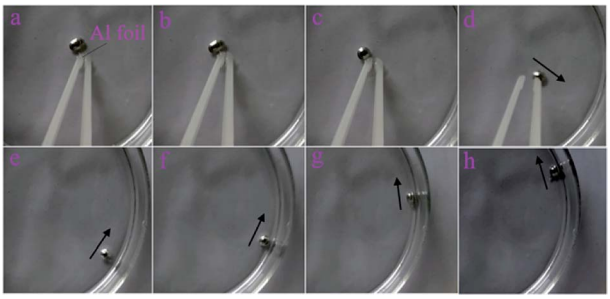

Fig. 4 Photographs of the process of aluminium foil instantaneous combined with mercury drop. Once the aluminium foil touched the mercury, they immediately moved together.

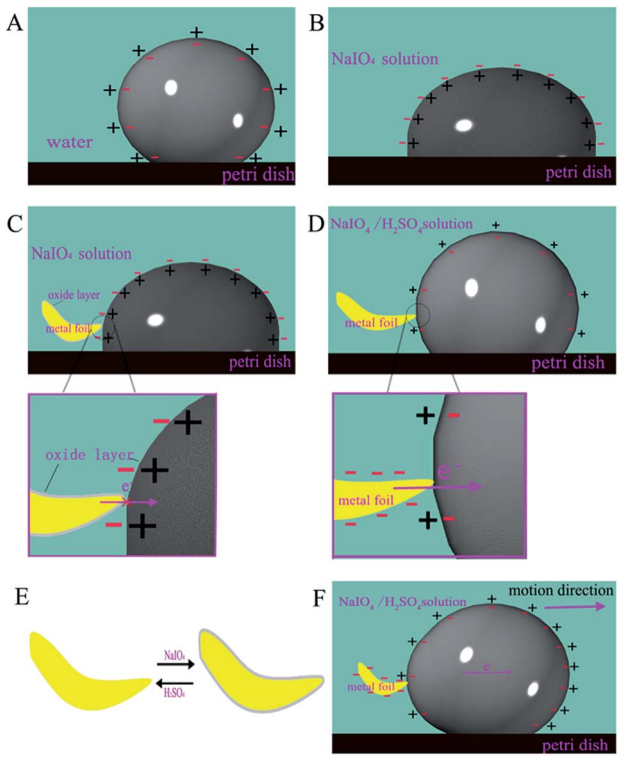

Fig. 5 Working mechanism of self-driven motor. (A) Schematic of electric double layer (EDL) model of mercury drops in water. (B) Schematic of the changed EDL structure of the mercury drop surface in NaIO4 solution. (C) The formation of the oxide layer of the metal foil and the mercury drop in the $NaIO_4$ solution. (D) Metal foil and mercury drop placing in the $NaIO_4/H_2SO_4$ solution. (E) Formation and dissolution of the oxide layer on the surface of the metal foil. (F) Schematic of charge redistribution and the varied shape of the mercury drop.

includes friction from the wall (F_w), the bottom of the dish (F_b) and the solution (F_s). In fact, the movement of the mercury was caused by F_d, which is the surface tension difference between the head and rear of the mercury drop. The surface tension difference was caused by the asymmetrical distribution of the charge on the surface of the mercury drop.[23] The asymmetrical distribution of the charge can be attributed to two aspects. When the aluminium foil connected with the mercury drop, the oxide layer on the surface of the mercury drop near the aluminium foil was reduced. The surface tension at this end (rear) of the motor transient increased owing to losing the oxide layer. Therefore, a pressure difference was produced. Apart from this redox reaction, an Al/Hg galvanic cell was formed using aluminium foil as the cathode and mercury as the anode. The direct connection of two electrodes leads to a short circuit. The internal electrons directly flowed from aluminium to mercury, and gathered more electrons near the aluminium (rear). The electron transfer changed the distribution of the charges across the EDL, causing the potential difference (V) along the mercury surface and causing the surface tension (γ) gradient of mercury to drop (Fig. 3F) according to Lippmann's equation:[32]

$$\gamma(V) = \gamma_0 - 1/2 \times cV^2$$

where c is the EDL capacitance, V is the electrical potential across the EDL and γ_0 is the maximum surface tension at $V = 0$. The large amount of negative charge in the rear leads to a greater surface tension at the rear of motor. Here, the $NaIO_4$ and H_2SO_4 played an important role in the process of electron transfer to construct the self-driven motor. The pH value was adjusted to observe its effect on the speed of the motor. The relationship between pH and velocity is shown in Fig. 6 (ESI Movie S6†) and a small range of pH 2–3 has a significant impact on the speed of the motor. Here, we used a bit of acid to promote the connection of mercury drops and aluminium foil rather than removing the mercury oxide layer as in previous reports.[25] In this work the mercury skin was mainly removed by aluminium foil. The previously reported redox driving mechanism was based on the electrical formation of a hydrophilic oxide layer.[21] This motor was driven by the surface tension gradient owing to the electron transfer in the redox reaction. The mechanism of electron transfer is different in the two environments ($NaIO_4/H_2SO_4$ and NaOH). The electron transfer in NaOH solution involved the dissolution of Al by NaOH solution promoting Al to lose electrons, and then the electron flow moved from Al to the mercury drop.[8] Thus, the mechanism of this self-driven mercury motor is different from the

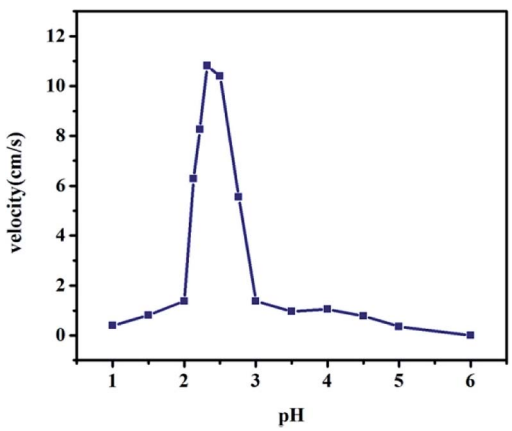

Fig. 6 The influence of pH on the self-driven motor.

mechanism that was previously reported. Herein, we present the possible mechanism of the motor as follows:

$$Hg + IO_4^- \rightarrow HgO + IO_3^- \quad (1)$$

$$2Al + 3IO_4^- \rightarrow Al_2O_3 + 3IO_3^- \quad (2)$$

$$Al_2O_3 + 6H^+ \rightarrow 2Al + 3H_2O \quad (3)$$

$$HgO + 2H^+ \rightarrow Hg^{2+} + H_2O \quad (4)$$

$$Hg^{2+} + 2Al \rightarrow 2Al^{3+} + Hg \quad (5)$$

$$2Al + 6H^+ + 3IO_4^- \rightarrow 2Al^{3+} + 3H_2O + 3IO_3^- \quad (6)$$

$$2Al + 3HgO + 6H^+ \rightarrow 2Al^{3+} + 3Hg + 3H_2O \quad (7)$$

3.3 Some interesting phenomena between the self-driven motors and mercury droplets

Dynamic behaviors between the self-driven motor (M_{A1}) and the liquid metal droplets that were not fuelled with aluminum (M) was observed. There were some interesting phenomena, such as pushing, colliding and bouncing between M_{A1} and M (Fig. 7, ESI Movie S7†). At the beginning, M_{Al} ran along the wall due to the self-driven force, and then M was pushed by M_{Al} along the wall when a head-on collision happened. However, the contact of M_{Al} and M was separated after they moved 1/3 round the dish together, and the direction of M_{Al} movement was opposite to the previously pushed direction. They acted like two colliding billiard balls because of the electrical repulsion (Fig. 8A). In the second collision was happened, M contacted with the aluminum foil that was connected with M_{Al}, which was similar to the process of the synthesis self-driven motor (Movie S7†). A system with two mercury drops on both ends of the aluminium foil was formed owing to the charge difference between the mercury drop and the aluminium foil (Fig. 8B). They were consolidated to a bigger droplet with aluminium foil present inside (Fig. 8C). Finally, it kept still on the same spot. We

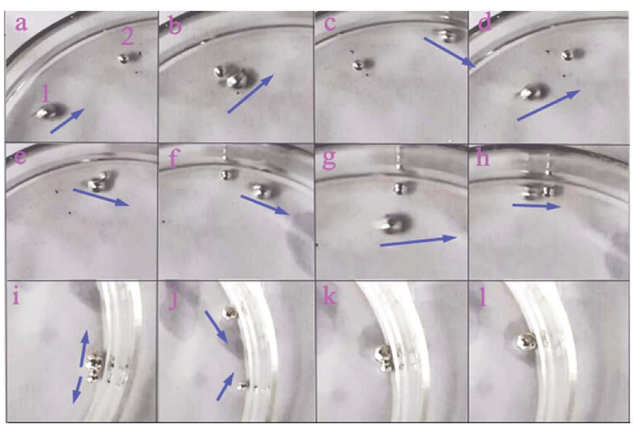

Fig. 7 The interaction of the self-driven motor and mercury droplet moving in $NaIO_4/H_2SO_4$ solution.

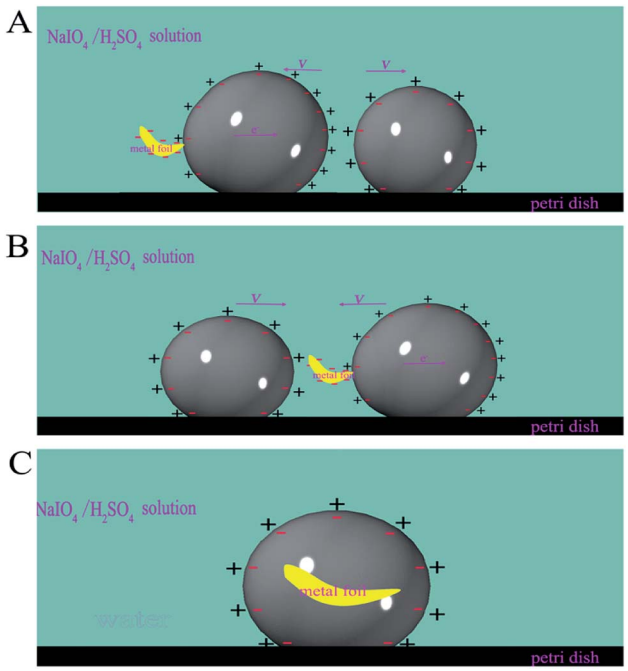

Fig. 8 Schematic of charge distribution of the interaction of the self-driven motor and mercury. (A) Repulsive interaction between mercury and mercury motor. (B) Mercury drop connected with the mercury motor through the aluminum foil. (C) Mercury drop and mercury motor were consolidated to a bigger droplet with aluminium foil present inside.

speculated that this phenomenon could be attributed to the formation of a charge balance on the surface of the mercury, which led to the disappearance of the pressure difference on the surface of the mercury (mentioned above); therefore, the self-driven property disappeared. The phenomenon proved that the self-driven property of the mercury droplet was caused by the potential difference on the surface of the mercury droplets.

3.4 Effect of other factors on the performance of the mercury motor

The performance of the motor was affected by several other factors, such as the volume of the motor, the temperature and the oxidant concentration. The volume of the mercury drop is an important factor that affects the speed of the mercury motor. As shown in Fig. 9(A and B), we observed the self-driven mercury motor ($D = 2$ mm and $D = 3.5$ mm) and found that the smaller diameter motor had a faster self-driven speed. According to the Young–Laplace equation,[33] the pressure jump can be represented as:

$$p = \gamma \times 2/r$$

where γ is the surface tension and r is the radius of the motor. Therefore, the surface tension γ will affect the final pressure jump between the water and the liquid metal object. In addition, the radius r also affects the pressure jump according to the equation. Therefore, different volumes of the motor present different speeds.

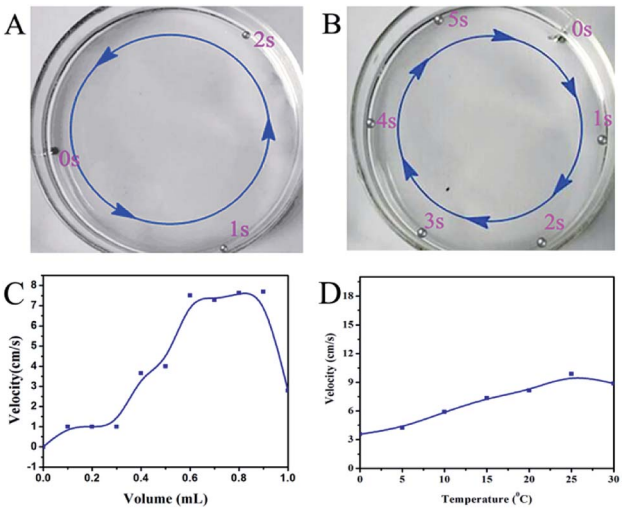

Fig. 9 Other factors affect on the performance of the mercury motor. (A) The movement of self-driven motor ($D = 2$ mm) along the wall of Petri dish. (B) The movement of self-driven motor ($D = 3.5$ mm) along the wall of Petri dish. (C) The influence of the self-driven motor by the volume of 0.05 M $NaIO_4$. (*D*) The speed of motor at different temperatures.

The concentration of the oxidant directly affects the speed of the mercury motor. Here, we explored the effect of the amount of oxidant on the motor velocity. As shown in Fig. 9C, with the addition of $NaIO_4$, the speed of the motor increased gradually. The speed was significantly improved when the volume of 0.05 M $NaIO_4$ was greater than 0.3 mL. It was found that the motor has a faster moving speed when the volume of the oxidant is 0.6–0.9 mL. We also investigated the effect of temperature on the motor. Mercury is volatile, so we chose 0–30 °C as the temperature test range. The relationship between velocity and temperature is shown in Fig. 9D; in a certain range, with the increase of temperature, the average velocity of the mercury motor will increase. However, with the further increase of temperature, the surface tension of the mercury drop decreased. Both the assembly and the driving of mercury motor were affected by temperature. So for the mercury motor, the temperature does not have a positive correlation with speed. According to our actual operation, the operating temperature of the motor is better in the range 15–25 °C.

4 Conclusions

In summary, we realized the controllable change of mercury droplet shape and discussed the contribution of the nail for merging of mercury droplets in oxidant solution. The surface tension, which determined the shape and state of the mercury drop, was changed by the oxidant and nails. Meanwhile, the self-driven system based on metal foil and a mercury drop was established in $NaIO_4/H_2SO_4$ solution, the speed of the self-driven motor reached 10 cm s^{-1}, and the mechanism of self-driven motion was investigated in this work. The results demonstrated that the self-driven force was caused by the potential difference on the surface of the mercury droplets, which is affected by the electronic transfer between the metal foil and the mercury drop. Besides, we confirmed that the optimum pH range is between 2 and 3. In addition, the collision and bouncing between the motor and another mercury drop was also investigated in this work. The mechanism of this self-driven mercury is different from that of the motor in the NaOH system, which dissolved aluminum in liquid metal without an oxidant. Finally, we investigated the factors that affect the performance of the mercury motor. The driving mechanism in this paper provides an idea for investigating self-driven mercury motors, promoting the development of robot design in the field of self-motion.

Acknowledgements

This work was supported by the National Natural Science Foundation of China (No. 21407109, 21377089).

Notes and references

1 J. Zhang, R. Guo and J. Liu, *J. Mater. Chem. B*, 2016, **4**, 5349–5357.
2 F. Mou, C. Chen, Q. Zhong, Y. Yin, H. Ma and J. Guan, *ACS Appl. Mater. Interfaces*, 2014, **6**, 9897–9903.
3 X. Yu, Y. Li, J. Wu and H. Ju, *Anal. Chem.*, 2014, **86**, 4501–4507.
4 D. Kagan, P. Calvo-Marzal, S. Balasubramanian, S. Sattayasamitsathit, K. M. Manesh, G.-U. Flechsig and J. Wang, *J. Am. Chem. Soc.*, 2009, **131**, 12082–12083.
5 W. Gao, A. Pei and J. Wang, *ACS Nano*, 2012, **6**, 8432–8438.
6 F. Mou, C. Chen, H. Ma, Y. Yin, Q. Wu and J. Guan, *Angew. Chem., Int. Ed.*, 2013, **52**, 7208–7212.
7 W. Gao, A. Uygun and J. Wang, *J. Am. Chem. Soc.*, 2011, **134**, 897–900.
8 J. Zhang, Y. Yao, L. Sheng and J. Liu, *Adv. Mater.*, 2015, **27**, 2648–2655.
9 X. Chen, G. Wu, T. Lan and W. Chen, *Chem. Commun.*, 2014, **50**, 7157–7159.
10 W. Gao, M. D'Agostino, V. Garcia-Gradilla, J. Orozco and J. Wang, *Small*, 2013, **9**, 467–471.
11 J. Zhang, L. Sheng and J. Liu, *Sci. Rep.*, 2014, **4**, 7116.
12 S.-C. Tan, H. Gui, B. Yuan and J. Liu, *Appl. Phys. Lett.*, 2015, **107**, 071904.
13 J. Zhang, Y. Yao and J. Liu, *Sci. Bull.*, 2015, **60**, 943–951.
14 T. Mirkovic, N. S. Zacharia, G. D. Scholes and G. A. Ozin, *Small*, 2010, **6**, 159–167.
15 J. Wang and W. Gao, *ACS Nano*, 2012, **6**, 5745–5751.
16 T. Toyota, N. Maru, M. M. Hanczyc, T. Ikegami and T. Sugawara, *J. Am. Chem. Soc.*, 2009, **131**, 5012–5013.
17 L. Sheng, J. Zhang and J. Liu, *Adv. Mater.*, 2014, **26**, 6036–6042.
18 M. R. Khan, C. B. Eaker, E. F. Bowden and M. D. Dickey, *Proc. Natl. Acad. Sci. U. S. A.*, 2014, **111**, 14047–14051.
19 A. F. Chrimes, K. J. Berean, A. Mitchell, G. Rosengarten and K. Kalantar-zadeh, *ACS Appl. Mater. Interfaces*, 2016, **8**, 3833–3839.
20 L. Wang and J. Liu, *Appl. Phys. Lett.*, 2016, **108**, 161602.

21 R. C. Gough, J. H. Dang, M. R. Moorefield, G. B. Zhang, L. H. Hihara, W. A. Shiroma and A. T. Ohta, *ACS Appl. Mater. Interfaces*, 2015, **8**, 6–10.
22 S.-Y. Tang, V. Sivan, K. Khoshmanesh, A. P. O'Mullane, X. Tang, B. Gol, N. Eshtiaghi, F. Lieder, P. Petersen and A. Mitchell, *Nanoscale*, 2013, **5**, 5949–5957.
23 S.-C. Tan, B. Yuan and J. Liu, *Proc. R. Soc. A*, 2015, **471**, 20150297.
24 X. Tang, S.-Y. Tang, V. Sivan, W. Zhang, A. Mitchell, K. Kalantar-zadeh and K. Khoshmanesh, *Appl. Phys. Lett.*, 2013, **103**, 174104.
25 M. Mohammed, R. Sundaresan and M. D. Dickey, *ACS Appl. Mater. Interfaces*, 2015, **7**, 23163–23171.
26 G. Lippmann, *Ann. Phys.*, 1873, **225**, 546–561.
27 D. K. Verma, H. Singh, A. Contractor and P. Parmananda, *J. Phys. Chem. A*, 2014, **118**, 4647–4651.
28 S. Demiri, M. Najdoski, V. Mirceski, V. M. Petruševski and D. Rosenberg, *J. Chem. Educ.*, 2007, **84**, 1292.
29 J. L. Ocampo-Espindola, E. Ramírez-Álvarez, F. Montoya, P. Parmananda and M. Rivera, *J. Solid State Electrochem.*, 2015, **19**, 3297–3303.
30 O. Schnitzer, I. Frankel and E. Yariv, *J. Fluid Mech.*, 2013, **722**, 394–423.
31 O. Schnitzer and E. Yariv, *Phys. Rev. E: Stat., Nonlinear, Soft Matter Phys.*, 2013, **87**, 059901.
32 J. Lee and C.-J. Kim, *J. Microelectromech. Syst.*, 2000, **9**, 171–180.
33 S.-Y. Tang, K. Khoshmanesh, V. Sivan, P. Petersen, A. P. O'Mullane, D. Abbott, A. Mitchell and K. Kalantar-zadeh, *Proc. Natl. Acad. Sci. U. S. A.*, 2014, **111**, 3304–3309.

